# In-Cylinder Measurement of Turbulence by Laser Homodyne Principle

Makoto Ikegami, Masahiro Shioji, Dao-Yuan Wei
and Masanori Sugiura
Faculty of Engineering
Kyoto University
Kyoto

ABSTRACT

A laser homodyne principle has been applied to measure turbulence within an engine cylinder. This method features a direct detection of relative fluid motion in a turbulent flow without relying upon the time-sequential data. Because of this advantage, cyclic variation biases that may be encountered at ordinary methods may be removed. The intensity fluctuation of laser light scattered from tracer particles has been measured using a photoelectron correlation technique by a high-speed digital correlator. Tests have been conducted at several engine speeds and swirl ratios at a motored engine. The results are satisfactory supporting the feasibility of the proposed method in measuring the turbulence intensity and the length scale. It has been shown that swirl not only enhances the turbulence intensity but also increases the length scale at the compression end. In addition, a discussion is given of the in-cylinder measurement of the swirl velocity by the present laser homodyne method.

## INTRODUCTION

The motion of gas in the engine cylinder greatly affects performance and pollutant formation in both spark-ignition and compression-ignition engines. For this reason, much effort has been expended in attempts to clarify the details of in-cylinder flow. Several measuring methods including hot-wire anemometry and laser Doppler anemometry have been applied for this purpose. Although these methods are well-suited to the measurement of mean velocities, difficulties are met when turbulence is measured. This is mainly because the time-sequential data obtained by these methods do not allow the complete discrimination of fluctuations due to turbulence from those in the main flow. Fluctuation relative to ensemble average does not give turbulence intensity because of cycle-to-cycle variations.

Removal of cyclic variation biases from the obtained velocity data has been attempted using several techniques during the data processing stage(1)-(5). Dent(1) used a high-pass filter to obtain net fluctuation from the hot-wire anemometer signal. Lancaster(2) proposed a non-stationary time-averaged analysis on the assumption that velocity fluctuation due to turbulence during a time interval is obtainable from the instantaneous velocity fluctuation around the ensemble average, subtracted by the time-average of the velocity fluctuation during the interval. Rask and others(4) employed window-implemented ensemble averaging with smoothed-ensemble data analysis to interpret their laser Doppler anemometry results. They also proposed a cycle-by-cycle analysis that eliminates the cyclic variation from the smoothed-ensemble data. A reasonable degree of success has been achieved in each method, but the assumptions included hamper the acquisition of reliable results of turbulence intensity and scale.

To eliminate these difficulties, there is a need for a new technique that allows the detection of turbulent motion directly without relying on time-sequential signal analysis. The present authors have explored the possibility of using the laser homodyne principle in measuring turbulence. This method features direct detection of relative fluid motion in the measuring volume by finding the light-intensity fluctuation due to beating from a scattering pair. This principle was first used by Bourke and others(6), but they gave no quantitative result. In a previous report(7), the present authors extended this method to obtain the theoretical background for measuring both turbulence intensity and spatial integral scale. They have also discussed the sources of errors and the accuracy of measurement. The present study applies this laser homodyne technique to the engine situation, to investigate the intensity and length of turbulence for various engine speeds and swirl ratios.

## PRINCIPLE AND THEORETICAL BACKGROUND

### Principle

Suppose a homodyne optical system in which scatterer particles suspended in a flowfield are illuminated by a thin laser beam, as is indicated in Fig.1. The scattered light is collected by a photomultiplier tube placed in the direction of $\alpha$ measured from the direction of the incident beam. In this situation, random particle motion due to turbulence causes a Doppler shift in frequency of the light scattered from an individual particle. Once the scattered light from two particles denoted by j and k is mixed when collecting light, a beat will be produced, and this frequency will

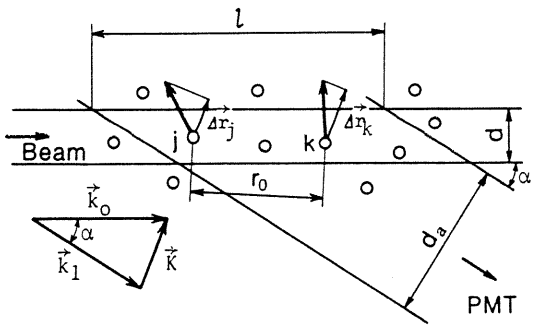


Fig.1 Diagram showing scattering geometry and the scattering vector

represent the relative velocity of the scattering pair. Thus the photomultiplier signal will represent the statistical average of the light beat over all pairs existing in the measuring volume. In other words, information on relative velocity may be obtained.

A practical method of processing the light beat received by the photomultiplier tube is to use either a digital correlator or a frequency analyser. In the present study, the former was used, yielding autocorrelation of light intensity fluctuation directly.

Autocorrelation of Light Intensity Fluctuation

To establish the foundation of this method, the autocorrelation of the light intensity fluctuation $R_I(\tau)$ where $\tau$ denotes time difference was obtained theoretically based on the theory of light beating and on the fluid mechanics of turbulence. The result of the analysis is outlined below. For details see the Appendix and previous report(7).

The autocorrelation of the scattered-light intensity fluctuation may be written as

$$R_I(\tau) = \langle I \rangle^2 \{1+G(\tau)\} \qquad (1)$$

where $\langle I \rangle$ denotes the average intensity of light and $G(\tau)$ the normalized signal part which can readily be read out from the correlator store. The problem is now reduced to formulating $G(\tau)$ by taking into account the turbulent fluid motion. To do this, the following assumptions were made.

(i) The scatterer particles have the same size and track the flow faithfully.

(ii) The turbulent flowfield is uniform and isotropic, at least within the measuring volume.

(iii) The probability density function of relative fluid position due to relative-turbulent diffusion is Gaussian.

(iv) The ensemble average of the square deviation of the distance between two particles having an initial separation by $r_o$ after the time $\tau$ elapses is(8)

$$\langle \Delta r^2 \rangle = 2 u'^2 \tau^2 \{1-\exp(-r_o/L)\} \qquad (2)$$

where u' denotes the root-mean-square velocity of turbulence, or simply turbulence intensity, and L

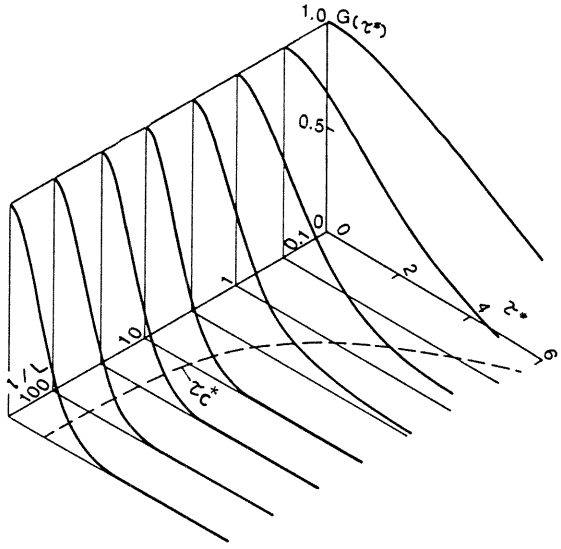


Fig.2 Theoretical autocorrelation coefficients for various ratios of $l/L$

the integral spatial scale of turbulence. Equation (2) would hold if $\tau$ is very small.

(v) The measuring volume has a rod-like shape of length $l$ which is sufficiently large compared with the beam diameter d.

On the above assumptions $G(\tau)$ was calculated for various ratios of the measuring length to the turbulence scale $l/L$. The complete form may be found in the Appendix. Figure 2 shows the results against non-dimensional difference time

$$\tau^* = (2/\sqrt{\pi})\, K\, u'\tau \qquad (3)$$

where K denotes the magnitude of the scattering vector $\vec{K}$. Using light wavelength $\lambda$, we find

$$K = (4\pi/\lambda)\sin(\alpha/2) \qquad (4)$$

As may be seen from Fig.2, $G(\tau^*)$ is close to a Gaussian distribution and the spread in $\tau^*$ direction increases with the decrease in $l/L$. At a very large $l/L$, the spread tends to be constant. The broken curve represents the non-dimensional integral characteristic time defind by

$$\tau_c^* = \int_0^\infty G(\tau^*)\, d\tau^* \qquad (5)$$

This value is close to unity at large $l/L$. To analyze the obtained data, it is convenient to use the fluctuation velocity as follows.

$$v = u'/\tau_c^* = (\sqrt{\pi}/2\, K)/\int_0^\infty G(\tau)\, d\tau \qquad (6)$$

In Fig.3 the v/u' value calculated is shown against $l/L$ (See c=0). As $l$ increases, v/u' first increases to 1/2 power and then approaches unity at a large $l/L$. This inclination coincides well with the results of experiments made for a pipe flow by Bourke and others(6) in a similar

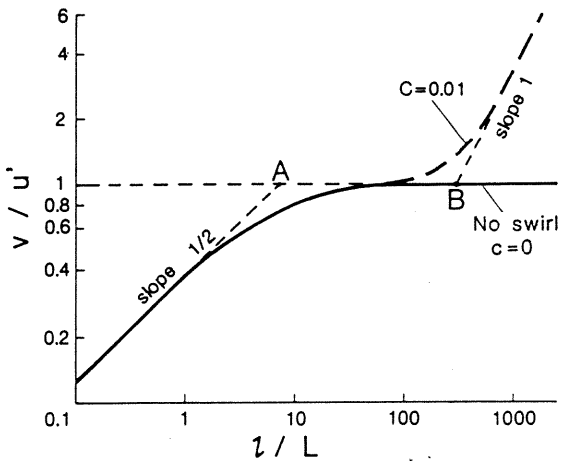


Fig.3 Theoretical relations between v/u' and $\ell$/L in the cases with and without swirl

homodyne technique. Using the obtained theoretical relation between v/u' and $\ell$/L, one can determine the turbulence intensity u' and the length scale L. The former may be found by obtaining v at a large $\ell$, say at twenty times the length scale L. The length scale L may also be determined by curve-fitting around point A in the figure. This method of finding u' and L turned out to be satisfactory judging from experiments made at a turbulent flow behind a grid in a steady pipe flow, as has been reported elsewhere(7).

Effect of Swirl

When a swirling motion is present, the fluctuation velocity at large value of $\ell$ no longer gives the turbulence intensity, if a forward scattering is employed. This is attributed to the fact that the gradient in the beam direction of the velocity component in the $\vec{K}$ direction affects the frequency of light beat from the scattering pair. This effect can be assessed theoretically(7). If the incident beam passes the center of a forced vortex having an angular velocity $\omega$, and if the scattered light is received in a purely forward direction ($\alpha$=0°), then the gradient is equal to $\omega$. To describe the effect of swirl, we use a parameter defined as

$$c = \omega L/u' \qquad (7)$$

In Fig.3 the v/u' curve in the case of c=0.01 is shown as an example. At point B the asymptote for the swirl effect intersects v/u'=1. As the angular velocity increases, point B shifts towards point A, and finally the two points overlap. In such a case, this technique for measuring the turbulence is no longer possible. However, if the swirl velocity is not so high when the points are well separated, the turbulence intensity u' can be estimated to some extent by curve-fitting around point A in the v versus $\ell$ relation. In addition, measurement of the mean swirl velocity may also be possible using the above principle, as will be discussed later.

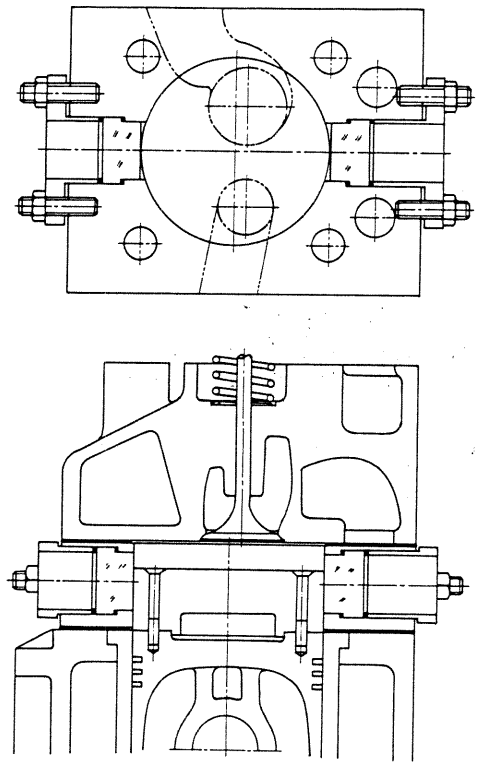

Fig.4 Cylinder head and piston arrangement

It should be noted that a backward-scattering optical system is entirely free from the effect of swirl. However, this system could not be used because of the limitation of the processing speed, as will be discussed later.

## EXPERIMENTAL APPARATUS AND PROCEDURE

Test Engines and Optical System

The proposed method was applied to study turbulence in a single-cylinder four-cycle, 102 mm bore, 106 mm stroke test engine having a flat piston and a compression ratio of 8.2:1. Four cylinder heads having different suction ports were used to produce various induction swirl ratios. The ratio denoted by $r_s$ was determined by an ordinary steady-flow rig test according to a proposed procedure(9). All measurements were conducted under motored conditions at two engine speeds of 400 and 800 rpm.

In Fig.4 the details of the engine head are shown. Optical access was made by inserting a spacer between the cylinder head and the liner. Two 40 mm diameter optical windows made of fused quartz were mounted in the spacer block having 50 mm in thickness. To compensate for the spacing, the piston was elongated by installing a metal disk on the original piston, thereby keeping the top clearance at 14.7 mm.

Figure 5 shows the schema of the experimental setup. A Spectra-Physics Model 164 argon-ion laser having a total light power of 2 W was used as the light source for the homodyne system. The beam passes through the quartz windows in the spacer. All optical equipment is installed on a

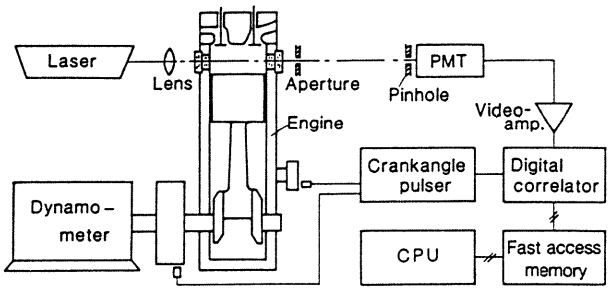


Fig.5 Experimental apparatus

flat movable bed. The bed is mounted on a traversing device which allows three-dimensional adjustment. Air-cushion mounts insulate the optical bed from engine vibration.

A laser beam was focused through one of quartz windows by a lens at the measuring position on a diametral line of the engine cylinder. Scattered light from tracer particles was detected in the forward direction of $\alpha$ ranging from 2.7° to 8.3° . The length of measuring volume $l$ was determined by an aperture placed just behind the window. The relation between the measuring length $l$ and the aperture diameter $d_a$ was

$$l = d_a/\sin \alpha \qquad (8)$$

To achieve the condition of coherency, the diameter of pinhole $d_p$ placed in front of a photomultiplier should satisfy (10)

$$d_a\, d_p/R < \lambda \qquad (9)$$

where R denotes the distance between the aperture and the pinhole and $\lambda$ the wavelength of the laser beam. R was set at 1.30 m.

To seed scatterer particles in the inlet air uniformly, a cyclone-type mixer was placed in a surge tank with a capacity of 50 L. The particle concentration was regulated by the flow rate of compressed air. The particles should be small enough in size to faithfully track the turbulent motion yet not so small as to produce an error owing to Brownian motion. For this reason, a titanium oxide powder having particle sizes between 0.2 μm and 0.4 μm was used.

To prevent the windows from being contaminated, the quantity of splash lubricant was minimized by keeping the oil-level in the crank case much lower than normal. In addition, the gas was evacuated from the crank case with a vacuum pump during tests to suppress the splashing of oil.

## Signal Processing

A Hamamatsu Photonics R464 type photomultiplier tube was used to detect scattered light. The scattered light signal from the photomultiplier tube was passed to a digital correlator in the form of pulse train after amplification and discrimination by a LeCloy MVL100TB type 170 MHz wide-band preamplifier. The correlator devised was a 12 bit 128 channel single-clipped digital correlator with a maximum clock speed of 50 MHz. This calculated directly the autocorrelation coefficients of the light intensity fluctuations(11). To sample data at a specified engine crank angle, input pulses to the digital correlator were gated during a crankangle window of 4° using a crankangle marker from the flywheel. To obtain each ensemble-averaged correlogram, ten cycles or more were necessary under typical measuring conditions.

The autocorrelation data acquired by the digital correlator were stored temporally in a Nihon-Kanomax 5211-1 type 256 kilobyte fast-access memory, to minimize the time of acquisition. This enabled measurements before the windows became contaminated. To extract the signal part from each autocorrelogram obtained, data reduction was made on a processing system consisting of a micro-computer and a Mitsubishi Melcom 70/20 mini-computer. A routine for a least-square fit to a Gaussian profile was included in the data processing.

## Measuring-volume Geometry

To optimize the optical setup under several restrictions imposed, care had to be taken in selecting the scattering angle $\alpha$ and the incident beam diameter d. The latter might be determined by a compromise between the minimum measuring length and the transit time error. To alleviate the transit time effect, a 500 mm lens was used to focus the beam having a waist diameter of 0.27 mm. When we consider a typical in-cylinder flow having a mean velocity of 20 m/s and a turbulence intensity of 4 m/s, the average transit time across the beam is 14 μs, while real characteristic time defined by the integral of $G(\tau)$ is 0.2 μs at $\alpha$=4.9°. In this case, the transit time error is sufficiently small because the characteristic time is an order of magnitude smaller than the transit time. The scattering angle $\alpha$ was decided primarily by the maximum clock speed of the correlator. In fitting the obtained correlogram to a Gaussian function, the necessary characteristic time would roughly be ten times the clock interval to remove a sampling error. If the fluctuation velocity is again 4 m/s for example, the scattering angle $\alpha$ should be less than 5° at the highest clock speed of 50 MHz for the mentioned situation. For this reason, $\alpha$ was typically selected to be 4.9° in the present experiments, and under some marginal conditions scattering angles $\alpha$ from 2.7° to 8.2° were used.

The use of such a small scattering angle and a finite beam diameter could cause an error due to a large discrepancy in the shape of the measuring volume from what we assumed in the theory. To see if this was not the case, the effect of these two factors on the probability density function of the inter-particle distance was assessed for the selected scattering angle and the beam diameter, based on a numerical calculation using a Monte Carlo method. The results show that even at a very small scattering angle of $\alpha$ =4.9° , the deviation in the pdf of the inter-particle distance is insignificant as long as the measuring length $l$ is maintained at ten times the beam diameter d. In other words, the 0.27 mm beam might safely be used to measure the velocity fluctuation at a measuring length down to $l$=2.7 mm.

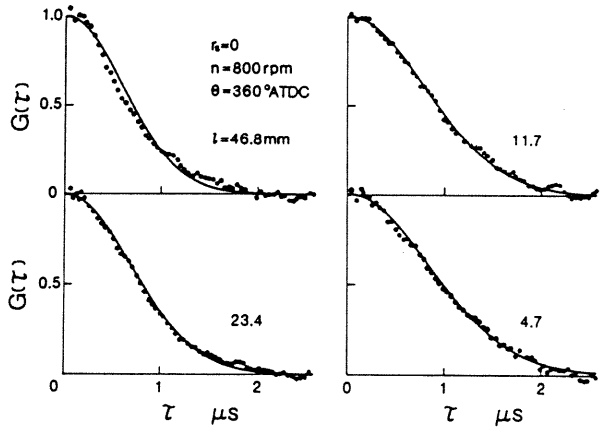


Fig.6 Examples of the autocorrelation coefficients obtained at different measuring lengths

EXPERIMENTAL RESULTS

Obtained Correlogram

Most of turbulence measurements in the engine cylinder were carried out at a depth of 10 mm measured from the cylinder-head surface. The horizontally-oriented measuring volume was centered on the cylinder axis throughout the study.

In Fig.6 a few examples of the obtained autocorrelograms are given in the normalized form of $G(\tau)$ for various measuring lengths $l$. They were collected at the above mentioned position under the no-swirl condition ($r_s$=0) at the top dead center of compression ($\theta$ =360°ATDC) at engine speed of 800 rpm. Each correlogram is close to a Gaussian profile as may be seen from a comparison with the Gaussian-fit curve in a solid line. It may also be noted that the spread of the curve in the $\tau$ direction decreases with $l$ in accordance with the theoretical prediction.

Similar measurements for various $l$ may give a set of correlograms for a single position and crankangle, thereby bringing about the relation between the fluctuation velocity v defined in Eq.(5) and the length $l$. In Fig.7 such relations are given for several crankangle $\theta$ under the no-swirl condition at n=800 rpm. The results are quite consistent with the prediction that v first increases with $l$ and then approaches a constant value that equals the turbulence intensity u'. Each line in the figure is the best fit to the theoretical v/u' versus $l/L$ relation already appearing in Fig.3. This curve fit will give the integral scale of turbulence.

In Fig.8 similar results for swirled cases are shown. They were obtained at the top dead center of compression at 800 rpm. The tendency of v against $l$ coincides well with the predicted effect of the swirl on the fluctuation velocity. In both cases, the presence of a swirl only affects v at a very large measuring volume, so that the turbulence measurement is possible.

Turbulence Intensity

To reveal the in-cylinder turbulence, measurements were carried out using this method for a variety of crankangles. First, the changes in

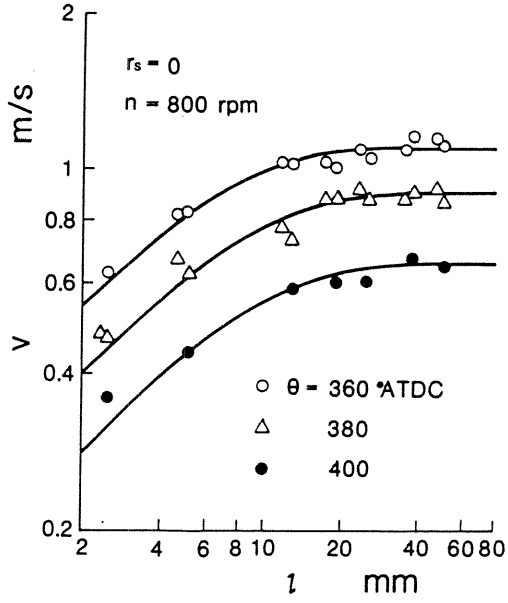


Fig.7 Fluctuation velocity against measuring length at no-swirl

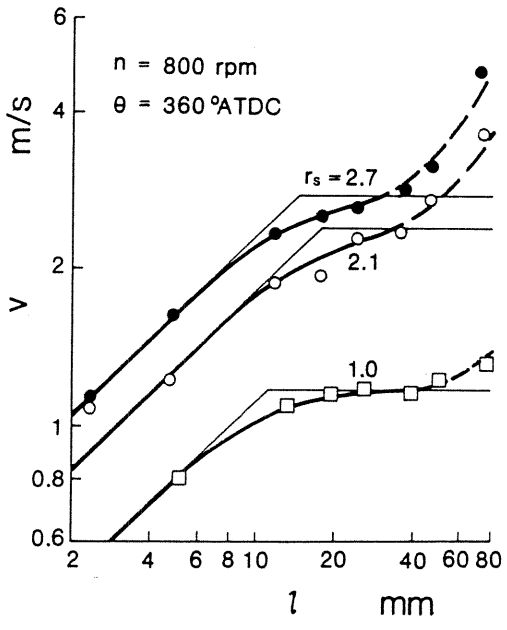


Fig.8 Fluctuation velocity against measuring length for different swirl ratios

the turbulence intensity u' with crankangle $\theta$ were investigated over whole cycles. The measuring length $l$ was 35.1 mm as a tentative choice. This made it possible to read out u' directly from the fluctuation velocity v, but a 10% error would be inevitable in the swirled cases. In Fig.9 the results obtained with and without swirl are shown for the engine speeds n=400 rpm and 800 rpm. In every case, just after the intake valve opens at $\theta$ =710° ATDC, the turbulence intensity

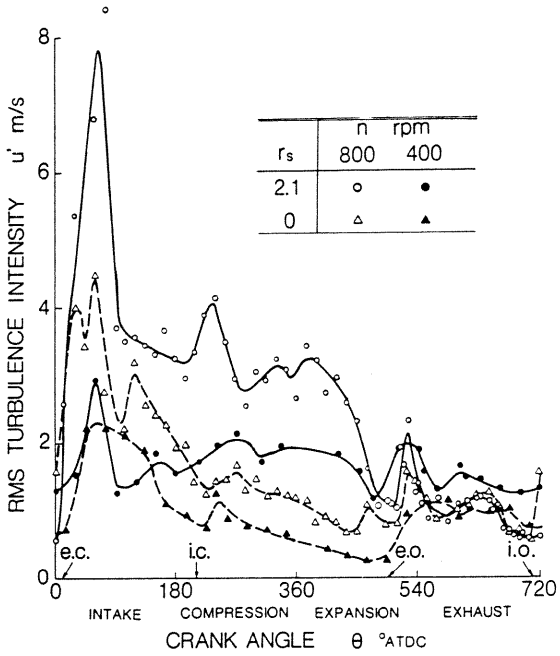


Fig.9 Course of turbulence intensity with crankangle at two engine speeds for the cases with and without swirl

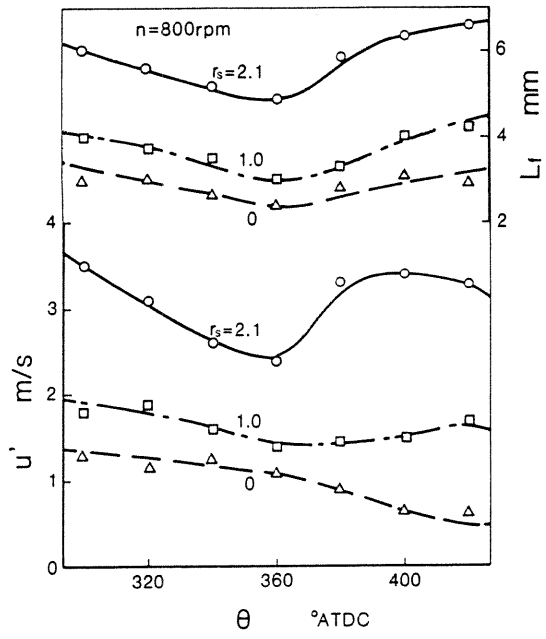


Fig.10 Turbulence intensity and length scale measured at three swirl ratios near compression end

u' increases rapidly as air flows into the cylinder. Between 70° and 80° ATDC when the piston velocity is the greatest, u' reaches the maximum. After the peak, u' quickly declines, possibly because of the quick change in the direction of the jet flowing through the intake valve as the piston moves downward. The turbulence intensity u' decreases slowly with the crankangle, until only a slight increase occurs when the intake valve closes at $\theta = 210°$ ATDC. At this stage, a highly directed flow passing through the intake valve would damp completely. During the compression and expansion strokes, u' decreases gradually showing oscillations, and finally reaches a small peak again when the exhaust valve opens at $\theta = 500°$ ATDC. In general, the observed changes are similar to those reported earlier(12).

Figure 9 indicates the effect of engine speed n on the in-cylinder turbulence. Except for the exhaust stroke, u' is almost doubled at every crankangle both with and without swirl. That the turbulence intensity is proportional to the engine speed is in accordance with the results reported by Witze(3).

It is striking to note from Fig.9, that the swirl largely increases u' at the same engine speed except for the later part of expansion stroke and the exhaust stroke. During the intake stroke, the turbulence intensity u' produced by an in-flow jet through a valve is much higher in the swirl case than in the no-swirl case. Especially in the swirl case, the decay of u' during the compression and expansion strokes is retarded so that a high level of turbulence intensity remains even after TDC during the expansion stroke. On the other hand, in the no-swirl case u' decreases monotonically with crankangle $\theta$. Presumably, this is partly because heterogeneously-distributed turbulent eddies are formed due to the complicated three-dimensional flows during intake period, and partly because of a large shear friction created by the swirl near the wall.

Further measurements were carried out focusing on turbulence intensity and length scale during the period around the end of compression. Figure 10 shows the obtained results for three swirl ratios $r_s$ at n=800 rpm. As may be seen from the figure, the turbulence intensity u' is largely dependent on $r_s$ and increases with $r_s$. While u' decreases monotonically with crankangle $\theta$ in the no-swirl case, the turbulence intensity begins to increase after TDC in both swirl cases. Presumably, this results from the fact that a stronger turbulence is produced near the wall due to swirl and is conveyed to the measuring position as the piston recedes from the cylinder head.

Since the one-point measurement did not indicate such a local production of turbulence near the wall of the cylinder head, measurements were made at several different distances from the cylinder head z. The obtained results are summarized in Fig.11. In the no-swirl case a monotonic decrease in u' with crankangle is seen at every position. On the contrary, at swirl ratio $r_s = 2.1$, a peak is seen in the u' curve after TDC at each position. As the measuring position is located closer to the cylinder head, the peak in u' after TDC is advanced and its peak level increases. This inclination may suggest that a wall-generated turbulence is conveyed downwards from the cylinder head with the piston motion. Having an irregular surface because of the exhaust and intake valves, the cylinder head might be a strong source of turbulence, in the case when a swirl is given. A similar effect was

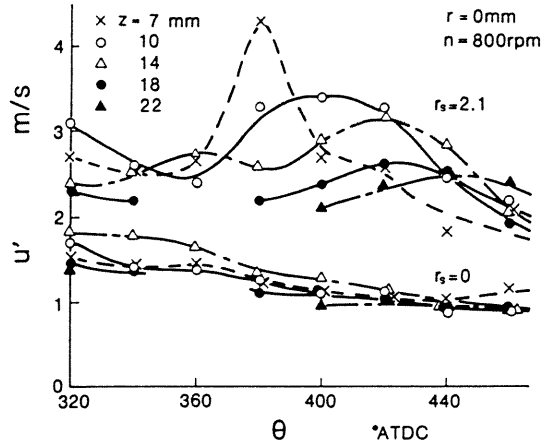


Fig.11 Turbulence intensity measured at various distances from cylinder head for the cases with and without swirl

reported by Dent(13), who pointed out that the wall shear flow plays an important part in turbulence production near the compression end.

Length Scale of Turbulence

Next, we see the length scale of turbulence in Fig.10. Since a forward-scattering system was used, the length scale L obtained was close to the transverse scale. Therefore, L was translated into a longitudinal scale $L_f$, namely

$$L_f = 2\,L \tag{10}$$

to enable comparison of the result with that gained by ordinary hot-wire anemometry. As may be seen from the figure, $L_f$ decreases with θ until TDC and then increases again. A minimum is reached at TDC and the $L_f$ profile after TDC looks roughly symmetrical against the TDC position excluding the case of $r_s$=2.1. This would imply that the scale is affected by a change in volume due to compression and expansion. It is also interesting to note that $L_f$ increases considerably with $r_s$; the minimum scale at $r_s$=2.1 is roughly twice that in the no-swirl case. It may be postulated that bigger turbulent eddies would postpone the decay of turbulence, causing a stronger turbulence to remain at later crank-angles. This might be responsible for the fact that the turbulence intensity is high when the swirl ratio is high. The reported values of $L_f$ near TDC vary depending on the engine size and the measuring method. Among them, the effect of the presence of swirl is reported possibly only by Lancaster(2), who observed that not only the turbulence intensity but also the length scale increased with the swirl produced by a shrouded intake valve. In spite of the swirl being produced in a different way, the obtained scales are almost identical in both experiments, suggesting that the turbulence near TDC is only slightly dependent on the intake process.

In-Cylinder Swirl Measurement

In the previous chapter, it has been shown

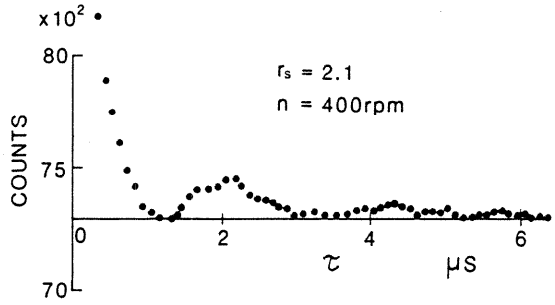


Fig.12 Oscillation due to swirl at a large measuring length

that the present homodyne method detects not only turbulent fluid motion but also a swirling motion. Based on this argument, we now consider the possibility of determining the swirl angular velocity. Two methods were conceived for this purpose in the forward-scattering homodyne mode in which the beam passes the center of the swirl having a rigid-body rotation. One is to detect the deviation point in the v versus $\ell$ curve at a large measuring length (See point B in Fig.3). For the cases of $r_s$=1.0, 2.1, and 2.7 in Fig.8, this method gave swirl ratios of 0.55, 1.17, and 1.61, respectively, at 800 rpm. These ratios correspond to 55 %, 56 %, and 60 % of the nominal swirl ratio, respectively, as determined by the steady-flow rig test.

The other method is more direct, making use of the oscillation superimposed on the correlograms. In Fig.12, such a correlogram is exemplified, each being obtained at a measuring length $\ell$=70.2 mm that is closer to the cylinder bore. The period of this oscillation may be related to the swirl angular velocity ω as may be seen below. Since the velocity fluctuation due to turbulence is negligible compared to that of the swirl at such a large measuring length, the probability density function of the inter-particle distance $r_o + \Delta r$ after a time difference τ for initial separation $r_o$ is described by a simple Delta function, namely

$$p(\Delta r, r_o, \tau) = \delta(\Delta r - \omega r_o \tau) \tag{11}$$

Using Eq.(A3) in the Appendix, we obtain

$$G(\tau) = \int_0^\infty dr_o Q(r_o) \int_{-\infty}^{\infty} \delta(\Delta r - \omega r_o \tau) \times \exp(-i K \Delta r)\, d\Delta r \tag{12}$$

Inserting Eq.(A7) into Eq.(12), we finally reach

$$G(\tau) = \frac{\sin^2(K\omega\ell\tau/2)}{(K\omega\ell\tau/2)^2} \tag{13}$$

This indicates that the correlogram is modulated by the oscillation having a period of $2\pi/(K\omega\ell)$. Thus, we can estimate ω from the first minimum point in the correlogram, and accordingly the in-cylinder swirl ratio is defined by

$$r_s' = 30\omega/(\pi n) \quad (14)$$

where n is engine speed expressed in rpm. When turbulence was taken into consideration, the period of oscillation did not differ much from that obtained assuming a laminar swirl. It turned out that for the port of $r_s$=2.1 the $r_s'$ at the compression end was 1.50 and 1.72 at 400 rpm and 800 rpm respectively. The port of $r_s$=2.7 gave 2.3 and 2.0 at 400 rpm and 800 rpm, respectively. Each in-cylinder swirl ratio is 15 % to 30 % lower than the nominal value of steady-rig test presumably due to the effect of wall friction. In the case of the port of $r_s$=1.0, it failed to measure the swirl velocity because no clear oscillation could be obtained at any measuring length.

There is a considerable disagreement between the swirl ratios obtained at two different methods. The reason is not clear, but probably the former method has underestimated the swirl ratio because of poor accuracy in determining the point at which swirl begins to affect fluctuation velocity when $l$ is increased. The present authors are convinced that the latter method of using oscillation is more reliable than the fluctuation-velocity method to determine the in-cylinder swirl ratio.

## CONCLUDING REMARKS

In the present study, the feasibility of the laser homodyne method for measuring the turbulence intensity and the length scale in a reciprocating engine was demonstrated. In principle, this method detects relative fluid motions without relying upon time-sequential data. Because of this advantage, some difficulties in the use of ordinary methods may be eliminated. However, the proposed method is not well-suited to detect localized properties of turbulence because a relatively large measuring volume has to be used.

The results obtained in a motored engine using the proposed method have shown that the course of the turbulence intensity with crank-angle is close to results reported earlier. A most interesting finding is that swirl not only enhances the turbulence intensity but also increases the length scale at the compression end. It is suggested that turbulence produced near the wall by a swirl motion can be conveyed downwards by the piston motion during the expansion stroke.

In the present study, a high-speed digital correlator was used to process the light-beat intensity fluctuations. However, the processing speed is not sufficient to measure strong turbulence that may be usual at higher engine speeds. Measuring such turbulence requires a faster correlator having a clock speed one order of magnitude higher than that employed in the present study. An alternate method of enhancing the processing speed would be the use of either a frequency analyser or a filter bank in place of the digital correlator. If such a fast processor is made available the proposed method may find a wider utilization.

## ACKNOWLEDGEMENTS

The authors wish to thank Dr. K. Miwa, Associate Professor of Kyoto University of Education, for his valuable support to this work.

This study was partially supported by Grant-in-Aid for Special Project Research (No.59110005) appropriated in 1984 by the Ministry of Education, Science and Culture.

## APPENDIX

The electric field induced at time t at the light detector by N particles is(14)

$$E(t) = \sum_{j=1}^{N} E_s \exp[\, i\{ \vec{K}\, \vec{r}_j(t) - \omega_o t\}] \quad (A1)$$

where $E_s$ is the amplitude contributed by each scatterer, $\omega_o$ the light frequency, $\vec{r}_j$ the position vector, $i$ the imaginary unit, and $\vec{K}$ the scattering vector (see Fig.1). The autocorrelation of the scattered-light intensity fluctuation is(10)

$$R_I(\tau) = \beta^2 \langle E(t)E^*(t)E(t+\tau)E^*(t+\tau)\rangle \quad (A2)$$

where $\tau$ denotes time difference, $\beta$ the constant for the optical system, $\langle\ \rangle$ the statistical average, and * the complex conjugate. If N is sufficiently large, the terms of scattering from each particle at a time and the terms arising from every particle pair during the time difference $\tau$ can remain, while all other uncorrelated terms vanish statistically. Thus $R_I(\tau)$ becomes the form of Eq.(1) consisting of the d.c. term due to simple radiation and the fluctuation term due to light beat. The signal part $G(\tau)$ may be described once we take into consideration the difference in relative position of each particle pair during $\tau$ (7). This leads to

$$G(\tau) = \langle \exp\{-i\, \vec{K}\Delta\vec{r}(\tau)\}\rangle \quad (A3)$$

where

$$\Delta\vec{r}(\tau) = \Delta\vec{r}_j - \Delta\vec{r}_k = \vec{r}_j(t+\tau) - \vec{r}_j(t) - \{\vec{r}_k(t+\tau) - \vec{r}_k(t)\} \quad (A4)$$

According to the assumptions, the probability of finding a change in inter-particle distance in $\vec{K}$ direction between $\Delta r \equiv |\Delta\vec{r}|$ and $\Delta r + d\Delta r$, for the particle pair having initial separation $r_o$, is

$$p(\Delta r, r_o, \tau)\, d\Delta r = (2\pi\langle\Delta r^2\rangle)^{-1/2} \times \exp\{-\Delta r^2/(2\langle\Delta r^2\rangle)\}d\Delta r \quad (A5)$$

For an infinite measuring volume, insertion of Eq.(2) and Eq.(A5) into Eq.(A3) gives

$$G(\tau) = \int_0^\infty dr_o \int_{-\infty}^{\infty} p(\Delta r, r_o, \tau)\exp(-i\,K\,\Delta r)\, d\Delta r = \int_0^\infty dr_o \exp[-K^2 u'^2 \tau^2\{1-\exp(-r_o/L)\}] \quad (A6)$$

For a finite length of measuring volume, the probability of $r_o$ should be taken into consideration. When the assumption (v) holds, namely $d \ll l$, the probability of finding an inter-particle length between $r_o$ and $r_o+\Delta r_o$ for a given measuring length $l$ is

$$Q(r_o)dr_o = \begin{cases} 2\, dr_o(l-r_o)/l^2 & [\ 0 \le r_o \le l\ ] \\ 0 & [\ r_o > l\ ] \end{cases} \quad (A7)$$

Multiplying Eq.(A5) by Eq.(A7) and inserting it into Eq.(A3), we have

$$G(\tau) = 2\int_0^{\ell} d(r_o/\ell)(1-r_o/\ell)\ \exp\left[-K^2u'^2\tau^2 \times\{1-\exp(-r_o/L)\}\right] \quad (A8)$$

Rewriting $r_o/\ell$ as $\xi$, we reach the final form as follows.

$$G(\tau) = 2\int_0^{1} d\xi\ (1-\xi)\ \exp\left[-K^2u'^2\tau^2 \times\{1-\exp(-\xi\ell/L)\}\right] \quad (A9)$$

Clearly $G(\tau)$ is a function of the turbulence intensity u', the integral scale of turbulence L, and the length of the measuring volume $\ell$. For the same value of $\ell/L$, the term of u' in $G(\tau)$ may be factored out. Thus normalizing $G(\tau)$ by the use of the non-dimensional time difference $\tau^*$ defined in Eq.(3), we can express the terms of u' and $\ell/L$ separately.

REFERENCES


1. Dent, J.C. and Salama, N.S., "The Measurement of the Turbulence Characteristics in an Internal Combustion Engine Cylinder," SAE Paper No.750886, 1975.
2. Lancaster, D.R., "Effects of Engine Variables on Turbulence in a Spark-Ignition Engine," SAE Trans. Vol.85, Paper No.760159, pp. 671-710, 1976.
3. Witze, P.O., "Measurements of the Spatial Distribution and Engine Speed Dependence of Turbulent Air Motion in an I.C. Engine," SAE Trans. Vol.86, Paper No.770220, pp. 1012-1023, 1977.
4. Rask, R.B., "Comparison of Window, Smoothed-Ensemble, and Cycle-by-Cycle Data Reduction Techniques for Laser Doppler Anemometer Measurements of In-Cylinder Velocity," ASME Meeting on Fluids Engineering, pp.11-20, 1981.
5. Wakisaka, T., Hamamoto, Y., Ohigashi, S., and Hashimoto, M., "Measurements of Air Swirl and Its Turbulence Characteristics in the Cylinder of an Internal Combustion Engine," Inst. Mech. Eng. Conference on Fuel Economy and Emissions of Lean Burn Engines, C91/79, pp. 51-62, 1979.
6. Bourke, P.J., et al., "A Study of the Spatial Structure of Turbulent Flow by Intensity-Fluctuation Spectroscopy," J. Phys. A Vol.3, pp. 216-228, 1970.
7. Ikegami, M., Shioji, M., and Wei, D., "Measurement of Turbulence by Laser Homodyne Technique," (in Japanese), Paper 85-0015A to be presented at Hokuriku Branch Meeting, JSME, July 11th, 1985.
8. Shirakashi, M., and Tomita, Y., "The Structure of Turbulent Diffusion (1st Report, Diffusion from a Source of Finite Width and Diffusion in a Mixing Region of Laminar and Turbulent Flows)," Bulletin of the JSME Vol.21 No.156, pp. 1000-1007, 1978.
9. Fitzgeorge, D., and Allison, J.L., "Air Swirl in a Road-Vehicle Diesel Engine," Proc. Inst. Mech. Engrs. (A.D.) No.4, pp.151-177, 1962-63.
10. Clark, N.A., Lunacek, J.H., and Benedek, G.B., "A Study of Brownian Motion Using Light Scattering," Am. J. Phys. Vol.38 No.5, pp. 575-585, 1970.
11. Schulz-Du Bois, E.O., "High-Resolution Intensity Interferometry by Photon Correlation," Photon Correlation Techniques, (Schulz-DuBois, E.O. ed.) Springer, pp.6-27, 1983.
12. Witze, P.O., "A Critical Comparison of Hot-Wire Anemometry and Laser Doppler Velocimetry for I.C. Engine Applications," SAE Trans. Vol.89, Paper No.800132, pp. 711-739, 1980.
13. Dent, J.C., and Salama, N.S., "Turbulence Structure in the Spark Ignition Engine," Inst. Mech.Engr. Conference on Combustion in Engines C83/75, pp. 23-32, 1975.
14. Cummins, H.Z., and Swinney, H.L., "Light-Beating Spectroscopy," Progress in Optics Vol.8, (Wolf,E. ed.) North-Holland, pp. 133-200, 1970.